NIH Public Access
Author Manuscript
Hear Res. Author manuscript; available in PMC 2012 May 1.

Published in final edited form as:
Hear Res. 2011 May ; 275(1-2): 30–42. doi:10.1016/j.heares.2010.11.011.

Rate-Level Responses in Awake Marmoset Auditory Cortex

Paul V. Watkins and **Dennis L. Barbour**
Laboratory of Sensory Neuroscience and Neuroengineering Department of Biomedical Engineering Washington University in St. Louis St. Louis, Missouri 63130, U.S.A.

Abstract

Investigations of auditory neuronal firing rate as a function of sound level have revealed a wide variety of rate-level function shapes, including neurons with nonmonotonic or level-tuned functions. These neurons have an unclear role in auditory processing but have been found to be quite common. In the present study of awake marmoset primary auditory cortex (A1), 56% (305 out of 544 neurons), when stimulated with tones at the highest sound level tested, exhibited a decrement in driven rate of at least 50% from the maximum driven rate. These nonmonotonic neurons demonstrated significantly lower response thresholds than monotonic neurons, although both populations exhibited thresholds skewed toward lower values. Nonmonotonic neurons significantly outnumbered monotonic neurons in the frequency range 6–13 kHz, which is the frequency range containing most marmoset vocalization energy. Spontaneous rate was inversely correlated with threshold in both populations, and spontaneous rates of nonmonotonic neurons had significantly lower values than spontaneous rates of monotonic neurons, although distributions of maximum driven rates were not significantly different. Finally, monotonicity was found to be organized within electrode penetrations like characteristic frequency but with less structure. These findings are consistent with the hypothesis that nonmonotonic neurons play a unique role in representing sound level, particularly at the lowest sound levels and for complex vocalizations.

Keywords

nonmonotonic; level-tuned; threshold; best level; dynamic range; monotonicity index; cortical column; marmoset monkey; primate

© 2010 Elsevier B.V. All rights reserved.

Please send correspondence to: Dr. Dennis Barbour Department of Biomedical Engineering Washington University One Brookings Dr., Campus Box 1097 Uncas Whitaker Hall Room 200E St. Louis, MO 63130, U.S.A. Tel. (314) 935-7548, Fax. (314) 935-7448 dbarbour@biomed.wustl.edu.

Publisher's Disclaimer: This is a PDF file of an unedited manuscript that has been accepted for publication. As a service to our customers we are providing this early version of the manuscript. The manuscript will undergo copyediting, typesetting, and review of the resulting proof before it is published in its final citable form. Please note that during the production process errors may be discovered which could affect the content, and all legal disclaimers that apply to the journal pertain.

Research Highlights

- Neurons tuned to sound intensity or level are the most common neurons in primary auditory cortex
- These neurons are the most sensitive neuronal class to low-intensity sounds
- These neurons are most common at frequencies where most vocalization energy resides
- Neuronal response patterns to sounds at different intensities is organized into cortical columns

NIH-PA Author Manuscript
NIH-PA Author Manuscript
NIH-PA Author Manuscript

NIH-PA Author Manuscript

NIH-PA Author Manuscript

NIH-PA Author Manuscript

Introduction

Nonmonotonic neuronal responses to sound level (also referred to as level-tuning), whereby neurons show a maximum firing rate in response to a particular intermediate sound level, have been reported in many species and at many stages in the auditory pathway. In the primary auditory cortex (A1) of mammals, varying methodologies for characterizing nonmonotonic neurons have resulted in a large range of percentages of nonmonotonic responses reported in different studies and have made direct comparisons challenging. Preparations that report a proportion of nonmonotonic neurons of 25% or greater in anaesthetized A1 include cat (Clarey et al., 1994; Heil et al., 1994; Nakamoto et al., 2004; Phillips, 1990; Phillips et al., 1981; Phillips et al., 1995; Phillips et al., 1994; Sutter et al., 1995; Sutter et al., 2003), rat (Doron et al., 2002; Polley et al., 2007), owl monkey (Recanzone et al., 1999) and bat (Suga, 1977; Suga et al., 1982), and in awake A1 include macaque (Pfingst et al., 1981), squirrel monkey (Shamma et al., 1985) and marmoset monkey (Sadagopan et al., 2008). At least one study in awake primate auditory cortex reports nonmonotonic percentages below 25% (Recanzone et al., 2000). Some of the variation between studies can potentially be explained by variability in reliance upon multiunit recordings, which could bias a sampled population toward the least selective (generally monotonic) neurons (Chen et al., 2010; Sutter et al., 1995). Although precise numerical estimates vary, the majority of these studies find a substantial proportion of level-tuned neurons in A1.

In the dorsal cochlear nucleus (DCN), type IV neurons have a fully nonmonotonic response type and are physiologically and likely morphologically distinct from type II/III neurons, which have a fully monotonic response type (Young et al., 2002). Neuronal responses to sound level in the inferior colliculus (IC) begin to show a range of monotonicities including hybrid types that are somewhere in between completely nonmonotonic or completely monotonic (Aitkin, 1991; Ramachandran et al., 1999; Rees et al., 1988; Rose et al., 1963; Ryan et al., 1978; Semple et al., 1985). Despite the emergence of a continuum of monotonicities in the auditory pathway downstream from DCN, the complete monotonicity distinction between type II/III and type IV neurons in the DCN has provided a historical rationale for classifying neurons at higher auditory centers into two distinct categories based upon their rate-level characteristics.

Auditory nerve fibers are exclusively monotonic in response to the sound level of a pure tone centered at each fiber's characteristic frequency (CF) (Kiang et al., 1965b). Because nonmonotonic responses are not present in the auditory nerve, they therefore must be created by neural circuitry in the central auditory system. Direct evidence of this phenomenon in areas beyond the DCN has also been reported by observation and manipulation of these circuits (Faingold et al., 1991; Sivaramakrishnan et al., 2004; Tan et al., 2007; Wu et al., 2006). The active creation and maintenance of level tuning implies that this response feature is potentially important for encoding of stimulus intensity or a related stimulus property. Additionally, animals trained in level discrimination tasks show an increased proportion of level-tuned neurons in A1 over control animals (Polley et al., 2006; Polley et al., 2004), implying that nonmonotonic level encoding also plays an important behaviorally-relevant role. Because of the prevalence and behavioral relevance of nonmonotonic responses at the level of A1, we decided to characterize several functionally relevant response properties of these neurons—including threshold, CF distribution and dynamic range—and compare them with those of monotonic neurons.

Here we present detailed results on responses of single A1 neurons to pure tones at different sound levels. The tones are presented separately, surrounded by a period of silence, so that neuronal adaptation to sound level does not play a large role in their responses. In general

NIH-PA Author Manuscript

NIH-PA Author Manuscript

NIH-PA Author Manuscript

we find a significant difference in neuronal thresholds and dynamic ranges between the monotonic and nonmonotonic populations across the frequency range of hearing for the species, even when the effect of variable frequency sensitivity is removed. Several related response properties varied across neuron type including best level as well as spontaneous and driven rates.. The finding of lower non-adapted thresholds in nonmonotonic neurons than in monotonic neurons supports the hypothesis that nonmonotonic neurons may be specialized for encoding low sound levels (Watkins et al., 2008; Watkins et al., 2010).

Materials and Methods

Electrophysiology

All animal procedures were approved by the Washington University in St. Louis Animal Studies Committee. A head cap consisting of stainless steel screws, titanium head posts and dental acrylic was affixed to the skull of each marmoset monkey (*Callithrix jacchus*) under isoflurane anesthesia and with aseptic procedures. Immediately following temporalis muscle removal during surgery, the vasculature running within the lateral sulcus became visible through the skull and its location was marked on the skull. This landmark allows later microcraniotomies (<1 mm diameter) to be drilled through the skull with a custom drill directly over auditory cortex (just inferior to lateral sulcus). Following surgery, the animals were allowed to recover sufficiently prior to beginning experiments. During experimentation, the animals were awake and sat upright in a custom, minimally restraining primate chair inside a double-walled sound-attenuation booth (IAC 120a-3, Bronx, NY) with their heads fixed in place by the head posts. The location of primary auditory cortex (A1) was identified anatomically using lateral sulcus and bregma landmarks and then confirmed physiologically by high driven rates (typically 20 – 70 spikes/s), short latencies (10 – 15 ms), robust responses to tones in middle layers and a cochleotopic frequency map oriented from low frequencies to high frequencies in the rostral to caudal direction parallel to lateral sulcus.

High-impedance tungsten-epoxy electrodes (~5 MΩ @ 1kHz, FHC, Bowdoin, ME) were advanced perpendicularly to the cortical surface within the microcraniotomies. Microelectrode signals were amplified using an AC differential amplifier (AM Systems 1800, Sequim, WA) with the differential lead attached to a grounding screw. Single-unit action potentials were sorted online using manual template-based spike-sorting hardware and software (Alpha Omega, Nazareth, Israel). When a template match occurred, the spike-sorting hardware relayed a TTL pulse to a DSP system (TDT RX6, Alachua FL) that temporally aligned recorded spike times (2.5 μs accuracy) with stimulus delivery. Raw waveforms were also bandpass-filtered at 300 – 5000 Hz and digitally sampled at 25 kilosamples/s (TDT RX6 24-bit ADC) for offline analysis. Both spike times and digitized raw waveforms were saved to hard disk on a PC running Microsoft Windows XP.

Acoustic stimuli were synthesized digitally online at approximately 100 kilosamples/s with custom MatLab software (MathWorks, Natick, MA). The stimuli were then passed through a digital-to-analog converter (TDT RX6 24-bit DAC), amplified (Crown 40W D75A, Elkhart, IN) and delivered to a loudspeaker (B&W 601S3, Worthing, UK) located 1 m directly in front of and aligned along the midline of the animal's head. Speaker output was calibrated so that the maximum sound level delivered was approximately 105 dB SPL with a flat frequency response (±5 dB) from 60 Hz to 32 kHz (B&K 4191 Microphone with 2669 Preamplifier, Nærum, Denmark).

NIH-PA Author Manuscript

NIH-PA Author Manuscript

NIH-PA Author Manuscript

Acoustic Stimuli

Single neuron action potentials were isolated and recorded in A1 as animals were presented with auditory stimuli. Because sound level tuning properties in A1 revealed with pure tones are correlated with properties revealed using flat-spectrum noise (Recanzone, 2000), pure tones were used to simultaneously assess frequency and level tuning for each cortical neuron. Each single unit was analyzed with tones delivered at its characteristic frequency (CF), the frequency eliciting the greatest response from the neuron within 10 dB of threshold. Rate-level functions were measured by pseudorandomly delivering 100 ms CF tones of different amplitudes, typically 11 amplitudes spaced by 10 dB from –15 to 85 dB SPL, separated by at least 650 ms of silence.

Rates were calculated for the rate-level function from a time window beginning at the absolute response latency and ending 100 ms later. Each stimulus amplitude was presented pseudorandomly 10 times, and the mean rate over these repetitions was used for construction of the rate-level curve. Absolute response latency was estimated from each neuron using an automated algorithm whose parameters were chosen empirically by noting how well the automated latency estimations compared to hand-estimated latencies. An overlapping peristimulus time histogram (PSTH) was calculated for the response to each sound level using a 20 ms spike window incremented in 2 ms steps. Time-points in the PSTH were aligned with the center time of the sliding spike window. Each PSTH was smoothed with a Gaussian kernel having a standard deviation of 4 ms, and a rate threshold was calculated as either 15% of the maximum over all PSTHs (one corresponding to each sound-level response), or 15% of the maximum of the current PSTH if the maximum of the current PSTH was greater than 15% of the maximum over all PSTHs. For each PSTH the first time point after stimulus onset that (1) had a positive slope and (2) was greater than or equal to this rate threshold was chosen as the latency. The absolute response latency for each neuron was then taken as the minimum of these latencies measured over all of that neuron's PSTHs.

Data Analysis

All neurons isolated in A1 that were responsive to tones and had positive driven rates (i.e., raw discharge rate minus spontaneous rate) at CF during the stimulus interval were analyzed. Rate-level functions were fit with a six-parameter, two-tailed split Gaussian function to evaluate response characteristics. The model was given as

$$r(l) = a \quad \exp\left[-\frac{(l-\mu)^2}{2\sigma_{low}^2}\right] + c_{low} \qquad \text{for} \quad l \le \mu$$

$$r(l) = a \quad \exp\left[-\frac{(l-\mu)^2}{2\sigma_{high}^2}\right] + c_{high} \qquad \text{for} \quad l > \mu,$$

where r is the discharge rate of the neuron as a function of sound level l. The parameters of the fit were a, μ, σ_{low}, c_{low}, σ_{high}, and c_{high}: a is the amplitude, μ is the best level, σ_{low}^2 is the low sound level variance, c_{low} is the low sound level offset, σ_{high}^2 is the high sound level variance and c_{high} is the high sound level offset. This model allowed the upper and lower dynamic ranges of nonmonotonic neurons to be fit separately, but monotonic functions could still be fit easily by ignoring the upper dynamic range parameters. The sum squared error between the data and model was minimized using nonlinear optimization (*fmincon* medium scale algorithm in MatLab). Because the model contained a discontinuity where the two Gaussians joined, model values falling between the fit data points could in some cases be considerably different from interpolated values. For this reason, the visually depicted model values were linearly interpolated from the fit data points. The result is an overfitted

NIH-PA Author Manuscript

NIH-PA Author Manuscript

NIH-PA Author Manuscript

representation of the original data, but one that eliminated spurious rate values quite successfully. This completely automated denoising procedure was particularly effective at providing quantitative estimates of threshold and saturation values that matched visual estimates for both monotonic and nonmonotonic neurons better than any other single technique we employed.

A comparison of the goodness of fit values (r^2) for the monotonic and nonmonotonic populations demonstrated that our results were not systematically biased by fitting the rate-level functions with a split Gaussian (Supplementary Figure 1). The distribution of r^2 values (median = 0.94; interquartile range = 0.11) over the entire neuronal population confirmed that our fitting procedure resulted in good fits overall for the rate-level functions. More importantly, no significant difference existed between the r^2 distributions for the monotonic and nonmonotonic populations for these fits ($p = 0.12$, Wilcoxon rank-sum test). In other words, the split Gaussian fitting procedure appeared to capture rate-level function behavior equally well for monotonic and nonmonotonic populations.

Threshold and saturation points were measured at 20% and 80%, respectively, of the maximum driven firing rate (i.e., discharge rate minus spontaneous rate) of the model functions linearly interpolated to the nearest dB. Spontaneous firing rate was averaged from time intervals when no audible stimulus was presented, typically 200 ms preceding stimulus onset. Threshold and saturation were also measured for the upper dynamic range of nonmonotonic neurons, but the 20% and 80% points in these cases were calculated relative to the response to the most intense sound presented (typically 85 dB SPL). Best level was also taken from the model-fitted and linearly interpolated curves as the sound level eliciting the maximum firing rate.

Monotonicity index (MI) refers to the degree of reduced spiking at higher stimulus intensities and was calculated from the fitted rate-level responses as:

$$MI = \frac{\left(rate_{\max\_level} - rate_{\text{spontaneous}}\right)}{\left(\max\left(rate\right) - rate_{\text{spontaneous}}\right)},$$

where rate is the fitted rate-level function, $rate_{max\_level}$ is the rate in response to the most intense sound presented and $rate_{spontaneous}$ is the spontaneous rate measured as indicated above. Neurons with MI less than or equal to 0.5 were classified as “nonmonotonic” and neurons with an MI greater than 0.5 were classified as “monotonic.” A similar metric of monotonicity has been used in previous studies (de la Rocha et al., 2008; Doron et al., 2002; Phillips et al., 1994; Recanzone et al., 2000; Sadagopan et al., 2008; Sutter et al., 1995; Sutter et al., 2003), but without subtracting the spontaneous rate. By subtracting spontaneous rate, our MI reflects a ratio scale (as opposed to simply an interval scale) and is not biased by potential systematic differences in maximum driven and spontaneous rates over the population. Additionally, negative MIs indicate neurons that are suppressed below their spontaneous rate at high sound levels, which is likely indicative of locally inhibitory processes.

Minimum population thresholds as a function of frequency were computed from the convex hull (Matlab *convhull* function) of the two-dimensional points represented by threshold and CF for each neuron. All neurons from all monkeys and across all hemispheres were used for this computation, thereby leading to a lower bound on the frequency-dependent threshold for this species. The boundary lines from the convex hull were linearly interpolated (in log space for frequency) to find the minimum threshold as a function of frequency (dotted line in Figures 2A,B). This value was subtracted from the minimum threshold for each neuron to

NIH-PA Author Manuscript

NIH-PA Author Manuscript

NIH-PA Author Manuscript

obtain residual threshold, which provided a fairer comparison of intensity coding across frequencies than did raw thresholds.

Relationships between many variable properties of rate-level functions were assessed with either Pearson correlation or Spearman rank correlation. Pearson correlation measures a strictly linear relationship between two variables, whereas the Spearman rank correlation measures any monotonic relationship (not necessarily linear) between the variables. Because the Spearman rank correlation is more sensitive in this regard, it was used in instances where we report that no significant relationship exists. Pearson correlation was used in instances were we report that a specific linear relationship exists.

A permutation test was utilized to assess whether rate-level features such as CF and MI were arranged non-randomly by electrode penetration, i.e., if these features were related between neurons recorded at different depths of the same electrode penetration. Because electrodes were advanced approximately perpendicularly to the cortical surface, significantly non-random arrangement of neurons at different depths provides evidence for a depth organization of the particular rate-level feature. Neurons were first grouped according to penetration, and only penetrations with at least two recorded neurons were included in this analysis. Although the permutation test can apply to any rate-level property, we discuss only MI here for illustration. For each penetration, the mean and standard deviation of neuronal MIs was calculated. Because we are interested in whether MI values recorded on the same penetration were similar to one another, we defined our test statistic for the permutation test as the mean of MI standard deviations from each penetration. For the permutation test, a random assortment of neurons was created with the same number of penetrations and the same number of neurons per penetration as in the original dataset. The same test statistic was calculated for the permuted set, and this was repeated 10 million times to create a distribution of test statistics (mean of the penetrations' standard deviations). Additionally, a sample permutation that was closest to the mean of the distribution was saved for later comparison. The original test statistic was then compared to the distribution. A *p*-value was calculated as the total number of distribution values that were less than or equal to the original test statistic, divided by the number of iterations (10 million). We chose 10 million iterations in order to obtain non-zero p-values in a tractable amount of time on the computer hardware available for analysis. Additionally, a *z*-score was calculated from the original test statistic, minus the mean of the test statistic distribution, divided by the standard deviation of this distribution.

Results

Altogether, 544 primary auditory cortex neurons from 12 hemispheres of 7 awake marmoset monkeys (*Callithrix jacchus*) were analyzed for sound level encoding properties in response to characteristic frequency (CF) tones. As expected, a wide variety of input-output functions with positive driven rates during the duration of the tone were recorded, including purely monotonically increasing functions, monotonically nondecreasing functions with saturation at high levels and nonmonotonic functions with a best level eliciting the highest spiking rates (Figure 1). The degree of input-output monotonicity was quantified for each neuron by a monotonicity index (MI) calculated on interpolated, curve-fit rate-level functions (see Methods). MIs of this population ranged from 1 (completely monotonic) to 0 (completely nonmonotonic, suppression to spontaneous rates at high levels) and beyond to about –0.4 (completely nonmonotonic, suppression below spontaneous rates at high levels). The smallest MI in our dataset was –0.72 and only 0.6% (3 / 544 neurons) had MIs less than –0.4, while 14% (78 / 544 neurons) had MIs less than zero. Threshold and saturation levels were determined as 20% and 80% of maximum firing rate above spontaneous rates, respectively, and formed the bounds of a conservative estimate of dynamic range attributed

NIH-PA Author Manuscript

NIH-PA Author Manuscript

NIH-PA Author Manuscript

to each neuron. Only one dynamic range was estimated for rate-level functions with MI > 0.5 (monotonic neurons); for rate-level functions with MI ≤ 0.5 (nonmonotonic neurons), however, both a lower dynamic range and an upper dynamic range were defined by separate threshold and saturation values. Lower dynamic ranges (blue for monotonic neurons and red for nonmonotonic neurons in Figure 1) were measured as the range of sound levels from threshold to saturation. Upper saturation and upper threshold for nonmonotonic neurons were determined at 80% and 20% of maximum firing rate above the response at the maximum sound level presented. Upper dynamic ranges (green in Figure 1) were measured as the range of sound levels from upper saturation to upper threshold.

Collectively, the distribution of monotonic neuron dynamic ranges spanned the full range of sound levels tested, suggesting that this subpopulation of neurons has sufficient diversity to encode a wide intensity range of hearing (Figure 2A). Even with limited neuronal sampling across all the frequencies of hearing for this species, a dependence of the lowest neuronal thresholds on CF is apparent in Figure 2. About half of these neurons had dynamic ranges of 20 dB or less, but the apparent population spread in dynamic ranges and the spread in thresholds likely enables monotonic neurons to encode sound levels across the full range of levels and frequencies tested. The distribution of nonmonotonic neuron lower dynamic ranges, on the other hand, collectively did not span the full range of levels tested (Figure 2B). This difference is due partially to lower thresholds in this subpopulation and narrower lower dynamic ranges (over 80% with lower dynamic ranges of 20 dB or less). If the upper dynamic ranges of these neurons are included, however, then the potential coding levels for this subpopulation of neurons matches that of the monotonic population. This finding is consistent with the apparent use of nonmonotonic upper dynamic ranges to encode sound level under dynamic stimulus conditions (Watkins et al., 2008; Watkins et al., 2010).

In order to make valid across-neuron threshold comparisons, the neuronal dependence of threshold upon CF apparent in Figure 2 was taken into account. This dependence is grossly consistent with the marmoset audiogram as measured with behavioral studies of tone thresholds in marmosets (Seiden, 1957), implying that the cortical distribution of thresholds is inherited from the auditory periphery. A larger proportion of nonmonotonic neurons was observed in the frequency range that also exhibited the lowest population thresholds, motivating the need for calculating residual thresholds. That is, if the dependence of threshold upon CF had not been removed from the threshold estimates, then this dependence alone would have biased nonmonotonic neurons toward lower thresholds relative to monotonic neurons. We estimated minimal population threshold dependence upon CF and removed that value from our threshold estimates (see Methods). This procedure created relative minimum thresholds of approximately 0 dB over all frequencies in our dataset (Figure 3A). The procedure did not fit the minimum thresholds perfectly, particularly in locations of higher threshold concavities or notches (for example from 250 Hz to 1 kHz in Figure 2A,B), but allowed for a relatively flat 0 dB minimum residual threshold measure for neurons at most frequencies without fitting small variations in minimum population threshold.

Both monotonic and nonmonotonic neurons were found with CFs distributed across the full frequency range of hearing for marmosets (Figure 3B). Out of the entire population, 56% (305 / 544 neurons) were classified as nonmonotonic (MI ≤ 0.5) and 44% (239 / 544) neurons were classified as monotonic (MI > 0.5). These values likely represent a lower bound on the relative proportion of nonmonotonic neurons because if a greater maximum sound level had been delivered, neurons with intermediate MIs would likely have exhibited further decreased rate responses and correspondingly lower MI values. Overall, more sampled neurons were tuned to the frequencies at which the marmoset is most sensitive, in the range from 6 to 13 kHz (Figure 3B). Significantly more nonmonotonic than monotonic

NIH-PA Author Manuscript

NIH-PA Author Manuscript

NIH-PA Author Manuscript

neurons were observed in the 4 kHz ($p = 1.7\times10^{-4}$, binomial test) and 8 kHz ($p = 8.2\times10^{-4}$, binomial test) frequency ranges where marmoset vocalization energy is common, and significantly fewer nonmonotonic neurons were observed in the 32 kHz frequency range ($p = 0.046$, binomial test), where vocalization energy is less common.

The distribution of monotonic residual thresholds (median = 23 dB, interquartile range = 28 dB) was found to be significantly different ($p = 7.2\times10^{-16}$, Wilcoxon rank-sum test) from the distribution of nonmonotonic residual thresholds (median = 12 dB, interquartile range = 15 dB). As seen in Figure 3C, the distribution of residual thresholds is not uniform for either population. Overall, residual thresholds are skewed toward lower values for both populations, with 75% (409 / 544) of the combined population having residual thresholds of 30 dB or less. Some of this skew is undoubtedly caused by the limited effective range of sound levels tested at the highest and lowest frequencies due to this species' audiogram, but the skew is still apparent even if one considers only residual thresholds in the range 0 to 40 dB, which can receive contributions from neurons having any CF. The skew is greater for the nonmonotonic population and results in the lower median threshold for these neurons. Monotonic neuron thresholds appear to be more nearly uniform than those of nonmonotonic neurons, however, and as a consequence extend over a wider range of sound levels. Only a small number of nonmonotonic neurons were found to have high thresholds. For neurons with residual thresholds greater than 60 dB only 17% (6 / 36 neurons) were nonmonotonic versus 83% (30 / 36 neurons) that were monotonic. Similar analysis made with a statistical definition of threshold (see Methods) revealed the same trends (Supplementary Figure 2).

A visual assessment of neuronal dynamic ranges independent of CF can be obtained by sorting neurons of each class by residual threshold and plotting their dynamic ranges (Figure 4). This depiction confirms that more nonmonotonic neurons have lower thresholds than monotonic neurons, reflecting the difference in residual threshold skew seen in Figure 3C. As also seen in Figure 2, the overall range of sound level spanned by neuronal dynamic ranges is similar between the two populations, as long as both the upper and lower dynamic ranges of nonmonotonic neurons are taken into account. More apparent in Figure 4 is that the nonmonotonic lower dynamic ranges appear to be narrower than both the monotonic dynamic ranges and the nonmonotonic upper dynamic ranges.

All dynamic ranges are also skewed toward lower values. In fact, of the combined population dynamic ranges (lower dynamic ranges for nonmonotonic neurons), 80% (433 / 544) span 30 dB or less. They also show the effect of the audiogram as seen for neuronal thresholds (Figure 2) since higher minimum absolute thresholds at the less sensitive frequencies force neurons at these frequencies to have smaller dynamic ranges for a given fixed maximum sound level (Figure 5A). Distributions of dynamic ranges (Figure 5B–C) show that the lower dynamic ranges (median = 11 dB; interquartile range = 8 dB) of the nonmonotonic population are significantly smaller ($p = 8.0\times10^{-22}$, Wilcoxon rank sum test) than the monotonic dynamic ranges (median = 22 dB; interquartile range = 25 dB). The nonmonotonic upper dynamic ranges, however, account for most of the sound levels spanned by nonmonotonic neurons (median = 15 dB; interquartile range = 17 dB). These three distributions were significantly different from one another ($p = 0$, Kruskal-Wallis test with Tukey-Kramer correction for multiple comparisons). Dynamic ranges from both populations can stretch across large spans of sound level regardless of residual threshold, and the combined population of dynamic ranges for monotonic neurons and lower dynamic ranges for nonmonotonic neurons is bounded by, but is not significantly linearly correlated with, residual threshold (n = 544; $p = 0.47$, regression F test). Some monotonic neurons near the threshold of hearing, for example, exhibit dynamic ranges that span almost the full range of hearing tested.

NIH-PA Author Manuscript

NIH-PA Author Manuscript

NIH-PA Author Manuscript

Up to this point, neurons in the study population have been classified into two groups according to the shape of their rate-level functions. While such an experimental distinction is historical (Aitkin, 1991; Pfingst et al., 1981; Phillips et al., 1981; Rees et al., 1988; Ryan et al., 1978; Semple et al., 1985; Sutter et al., 1995), it does not capture the full variety of the rate-level functions depicted in Figure 1. In order to generalize the findings reported so far, we also compared each neuron's rate-level response properties directly with the degree of monotonicity as measured by MI. Figure 6, for instance, depicts a scatterplot of MI and residual threshold. We found a significant correlation between residual threshold and MI using a linear regression fit over all MI values greater than –0.4 ($r^2 = 0.15$; $p = 0$, regression F test, black line in Figure 6). Only 3 / 305 neurons had MIs less than –0.4 (minimum MI was –0.73), and these outliers were removed to avoid an inappropriate influence on the regression. The significant correlation remained when the regression was calculated for monotonic neurons only (MI > 0.5; $r^2 = 0.13$; $p = 1.3\times10^{-8}$, regression F test), but not for nonmonotonic neurons only (MI ≤ 0.5; $p = 0.91$, Spearman rank correlation test). In other words, the highest residual thresholds are disproportionately concentrated within the subpopulation of neurons that exclusively saturate their rate response at the highest intensities. This trend is most clear when considering only neurons with MI less than 1. The regression over these nonsaturating neurons is still significant, but with a much smaller correlation (MI < 1; $r^2 = 0.037$; $p = 2.9\times10^{-5}$, regression F test).

A large proportion of monotonic neurons (31% or 74 / 239 neurons) exhibited response rates that did not decrease at higher sound levels, corresponding to an MI of 1. The top left neuron in Figure 1 is an example of such a neuron. This subpopulation by itself had a median residual threshold of 42 dB, with individual values spanning nearly the full range of residual thresholds. This wide range of residual thresholds is particularly noteworthy because 60% of all neurons measured with residual thresholds greater than 40 dB have an MI of exactly 1. The traditional definition of MI without subtraction of spontaneous rates (see Methods) gave a qualitatively similar distribution as our revised definition of MI, but with more neurons clustered at the extremes of 0 and 1 (Supplementary Figure 3). Among the nonmonotonic neurons, 26% (78 / 305 neurons) had MIs (with the definition used in this study) less than 0, indicating suppression below spontaneous rate at the highest intensities.

In the cochlear nucleus, neurons with highly monotonic rate-level functions (Type IV) characteristically have relatively high spontaneous firing rates, and some nonmonotonic neurons (Type II) typically have relatively low spontaneous rates (Nelken et al., 1997; Spirou et al., 1999). Here we questioned whether a similar relationship exists for cortical neurons. MI and spontaneous rate of all neurons in the dataset were modestly correlated ($r = 0.09$; $p = 0.035$, Spearman rank correlation test), and distributions of spontaneous rate were significantly different ($p = 0.014$, Wilcoxon rank sum test) between monotonic (median = 2.5 spikes/s) and nonmonotonic (median = 1.6 spikes/s) neurons. Neurons demonstrated an inverse correlation between residual threshold and spontaneous rate (Figure 7), similar to findings in auditory nerve fibers (Kiang et al., 1976; Kiang et al., 1965a; Liberman, 1978; Rhode et al., 1985). While a linear regression of the cortical neurons revealed a significant relationship ($r^2 = 0.026$; $p = 1.5\times10^{-4}$, regression F test), the magnitude of the phenomenon appears to be smaller than that seen in auditory nerve. No significant correlation was apparent between dynamic range and spontaneous rate ($p = 0.90$, Spearman rank correlation test), contrary to findings in the auditory nerve (Schalk et al., 1980). Spontaneous rates were approximately log normally distributed (Figure 7B), except for a cluster of neurons with spontaneous rates measured to be zero (12 / 239 monotonic and 14 / 305 nonmonotonic). A log-normal distribution of spontaneous rates in primary auditory cortex has been previously reported (Hromadka et al., 2008).

NIH-PA Author Manuscript

NIH-PA Author Manuscript

NIH-PA Author Manuscript

Dividing the neuron population into three similarly sized groups with low (rate ≤ 0.95 spike/s), medium (0.95 < rate ≤ 4 spikes/s) and high (rate > 4 spikes/s) spontaneous rates (Figure 7C–E) revealed significantly different residual thresholds in pairwise comparisons among all groups ($p = 0$, Kruskal-Wallis test with Tukey-Kramer correction for multiple comparisons). The median residual threshold for the low, medium and high spontaneous groups was 23 dB, 16 dB and 12 dB, respectively. Just as in the auditory nerve, low-spontaneous spiking cortical neurons appear to encode higher sound levels. Threshold and spontaneous rate were still negatively correlated within both the monotonic ($r^2 = 0.026$; $p = 0.012$, regression F test) and the nonmonotonic ($r^2 = 0.069$; $p = 3.6\times10^{-6}$, regression F test) subpopulations. Given that (1) MI and threshold were positively correlated, (2) MI and spontaneous rate were positively correlated, one might intuitively *not* expect that (3) threshold and spontaneous rate would be negatively correlated, as we found. As reported above, within the subpopulations of monotonic and nonmonotonic neurons, a significant correlation between MI and threshold was only present for monotonic neurons. Thus, one could reconcile this lack of correlation transitivity if the relationship between threshold and spontaneous rate were only present within the nonmonotonic subpopulation, but as stated above, this was not the case. Ultimately and counter-intuitively, correlation is not necessarily a transitive relationship (Langford et al., 2001).

Our finding of significant differences in spontaneous rate between monotonic and nonmonotonic neurons led us to investigate whether this finding extended to the discharge rate from stimulation as well. The dataset did not reveal a correlation between monotonicity index and maximum discharge rate ($p = 0.13$, Spearman rank correlation test, Figure 8A). Likewise, no significant difference was observed between the distributions of maximum discharge rate for monotonic (median = 35 spikes/s; interquartile range = 49 spikes/s) and nonmonotonic (median = 36 spikes/s; interquartile range = 49 spikes/s) neurons ($p = 0.48$, Wilcoxon rank-sum test, Figure 8B). The driven rate of a neuron in response to a stimulus is its discharge rate minus its spontaneous rate, i.e., the amount that the neuron is excited above spontaneous firing. No significant difference in distributions of maximum driven rates existed for the two subpopulations ($p = 0.60$, Wilcoxon rank-sum test), both having median driven rates of 32 spikes/s. Similar to spontaneous rates, distributions of maximum discharge rates and maximum driven rates were also approximately log normally distributed. A substantial and highly significant correlation between spontaneous rate and maximum driven rate existed ($r^2 = 0.46$; $p = 2.2\times10^{-74}$, regression F test). Thus, neurons with greater spontaneous rates often had higher driven rates, irrespective of their monotonicity. Recall, however, that nonmonotonic neurons exhibited significantly lower spontaneous rates than monotonic neurons.

Other significant trends were consistent with those reported above. Although dynamic range is necessarily bounded by best level (BL), neurons with any particular residual BL demonstrated a variety of dynamic ranges (Figure 9A). This finding is consistent with the lack of correlation between threshold and dynamic range, as reported above. Residual BL was calculated by removing the approximate effect of frequency on the overall neuronal sensitivity, in the same fashion as for threshold (see Methods). For completely monotonic neurons (MI equal to 1; 74 / 239 monotonic neurons), the BL was the same as the maximum sound level presented. The BL distribution for monotonic neurons (median = 66 dB; interquartile range = 50 dB) was much more nearly uniform than that for nonmonotonic neurons (median = 30 dB; interquartile range = 30 dB), and these two distributions were significantly different ($p = 3.8\times10^{-32}$, Wilcoxon rank-sum test, Figure 9B). Consistent with the result for residual thresholds, a significant correlation existed between MI and BL for monotonic neurons ($r^2 = 0.33$; $p = 3.0\times10^{-22}$, regression F test) but not for nonmonotonic neurons ($p = 0.14$, Spearman rank correlation test). Finally, MIs were significantly positively correlated with dynamic ranges of monotonic ($r^2 = 0.13$; $p = 1.3\times10^{-8}$, regression

NIH-PA Author Manuscript

NIH-PA Author Manuscript

NIH-PA Author Manuscript

F test) and nonmonotonic ($r^2 = 0.14$; $p = 0.015$, regression *F* test) neurons. This trend was not surprising based upon the fact that monotonic and nonmonotonic neurons exhibited significantly different distributions of dynamic ranges (Figure 3B). A significant negative correlation was found between MI and upper dynamic range for nonmonotonic neurons, but this correlation could easily be an artifact of the fixed maximum sound levels presented.

In order to investigate whether neurons were organized by depth with regard to MI, we separated them into groups that were recorded at different depths of a single electrode penetration. Electrodes were always advanced roughly perpendicular to the cortical surface; thus neurons recorded at different depths approximately represent neurons in different layers of the same cortical column. Between two and seven neurons were recorded at different depths in each of a total of 149 penetrations, encompassing 435 / 544 neurons in the dataset. Just over half (78 / 149) of the penetrations consisted of two neurons only. To validate our recording and analytic techniques, we first verified that CF was non-randomly organized by electrode penetration. Frequency is known to be organized in a columnar fashion within A1 (Abeles et al., 1970). A sorted plot of mean ± standard deviation of neuronal CFs within each of the 149 penetrations is depicted in Figure 10A, demonstrated this organization.

In order to assess if the CF standard deviation within a penetration was significantly smaller than the standard deviation of neurons selected across penetrations, a permutation test comparing the actual penetrations with novel penetrations consisting of randomly permuted neurons was utilized. The permutation test resulted in an empirical distribution of the test statistic (in this case the mean of the penetration standard deviations) upon resampling across penetrations (see Methods). As expected, CF was much more similar within penetrations than across penetrations ($p < 1.0\times10^{-7}$, permutation test). In this case, the permutation test did not result in a single instance where the test statistic was less than that of the actual penetrations, so the *p*-value from the permutation test is an upper bound based upon the total number of permutation test iterations (10 million). For this reason, and to obtain an assessment of the degree of depth organization, we also ordered the actual penetrations by standard deviation (Figure 10B) and compared with one instantiation from one permutation iteration that resulted in a test statistic near the mean of the test statistic distribution. The plot is marked with the mean standard deviation of the penetrations for the actual data and for the representative instantiation from the permutation test. The representative instantiation mean is also shown with an error bar representing the standard deviation of the test statistic distribution. The *z*-score of the actual penetrations' test statistic is –11 relative to this distribution. The MI variation was much higher than CF variation across depths within each penetration, with the possible exception of very nonmonotonic and very monotonic subpopulations (Figure 10C). The within-penetration standard deviations are obviously greater than was observed for the case of CF, but they also exhibit significant organization ($p = 2.1\times10^{-6}$, permutation test). Sorted standard deviation of the MI penetrations was less than that of a near-mean representative instance from the permutation test (Figure 10D; *z*-score of mean standard deviation = –4.5). This difference was much less than that for CF. Thus, although depth organization of neuronal MI has a much greater variance than that of neurons' CF, a significant non-random correlation of MI exists between neurons in different layers of the same cortical column.

Discussion

The relatively high percentage of level-tuned or nonmonotonic sound level responses in the auditory system, their absence in auditory nerve fibers and their relatively low numbers in other sensory systems collectively raise the question as to what functional role they play in sound level representation and transformation. In this study of tone-responsive neurons in awake marmoset monkey primary auditory cortex (A1) using tone stimuli separated by

NIH-PA Author Manuscript

NIH-PA Author Manuscript

NIH-PA Author Manuscript

periods of silence, we made the following discoveries: (1) Nonmonotonic neurons have significantly lower minimum thresholds than monotonic neurons, even when accounting for characteristic frequency (CF). Furthermore, the amount of on-CF inhibition inferred from the monotonicity index (MI) is correlated with minimum threshold. There is no *a priori* reason to believe that these two neuronal characteristics would be related. (2) Both monotonic and nonmonotonic neurons have minimum thresholds skewed toward lower sound levels. (3) Larger percentages of nonmonotonic neurons were found from about 6 to about 13 kHz. This range also corresponds with the most energy in marmoset vocalizations (DiMattina et al., 2006). (4) Nonmonotonic neurons have significantly smaller lower dynamic ranges than monotonic neurons and both are clustered below about 30 dB. Still, many monotonic neurons' dynamic ranges and the combination of nonmonotonic neurons' upper and lower dynamic ranges span the full range of sound levels tested. (5) Residual threshold and spontaneous rate are inversely correlated over the entire population of monotonic and nonmonotonic neurons. This same finding has been noted previously in auditory nerve fibers (Kiang et al., 1976; Kiang et al., 1965a; Liberman, 1978; Rhode et al., 1985), so it is possible that this property is inherited largely or partly from subcortical inputs. (6) Spontaneous rates are significantly greater in the monotonic population than in the nonmonotonic population, but maximum discharge rates are not significantly different between these populations. All rates are log-normally distributed. (7) Neuronal MI is organized by depth, although not with as much order as CF. Our finding of a depth organization does not necessarily suggest that a significant laminar organization of MI exists, and we have not provided evidence here for or against a hierarchical organization of MI between lamina. Thus we refer to this finding in the current study as a depth organization instead of as a columnar organization of MI.

The relationship between minimum threshold and CF that was regressed out to calculate residual thresholds has been reported previously in many studies (Cheung et al., 2001; Imaizumi et al., 2004; Philibert et al., 2005; Recanzone et al., 1999). Our finding of significantly lower residual thresholds for cortical nonmonotonic neurons when compared with monotonic neurons is consistent with results reported in cochlear nucleus (Spirou et al., 1991; Young et al., 1976), IC (Aitkin, 1991; Ramachandran et al., 1999) and at least one report from anaesthetized auditory cortex (Sutter et al., 1995). Cortical monotonic neurons exhibit a more nearly uniform distribution of thresholds than nonmonotonic neurons, which tend to have thresholds clustered near hearing threshold. Type V/I thresholds in IC are also more uniformly distributed than Type O thresholds, which tend to be clustered toward lower values (Ramachandran et al., 1999). Lower thresholds for nonmonotonic neurons imply that they are not simply monotonic neurons with inhibition added at higher intensities (in which case thresholds would be expected to be similar for the two populations). Nonmonotonic neurons throughout the auditory system appear to inherit information preferentially arising from the most sensitive auditory nerve fibers. The careful preservation of this information all the way to auditory cortex in a consistent neuronal type implies that level-tuned neurons are involved in a fundamental auditory processing task.

Distributions of best-level (BL) for monotonic neurons in the current study were fairly uniform, except with a cluster at the highest levels. Nonmonotonic neurons, on the other hand, had BLs clustered at lower sound levels. At least one study in A1 has reported results suggesting that BLs are clustered at or below 40 dB SPL (Phillips et al., 1994). Other studies in A1 have reported either an apparent clustering of BLs at the highest intensities (Polley et al., 2007; Recanzone et al., 2000; Recanzone et al., 1999) or a more nearly uniform distribution of BLs (Heil et al., 1994; Sadagopan et al., 2008). Because we included all neurons encountered with any driven response to tones and used search stimuli including all frequencies and sound levels, we isolated many nonmonotonic neurons with a range of characteristics, all of which are represented compactly in Figure 4. Differences in search

NIH-PA Author Manuscript

NIH-PA Author Manuscript

NIH-PA Author Manuscript

stimuli and sampling between the current study and Recanzone et al. (2000), also from awake primate A1, have been highlighted previously by Sadagopan and Wang (2008). These differences could account at least partially for differences in spontaneous and driven rates between nonmonotonic type neurons we sampled and similar neurons sampled by(Recanzone et al., 2000).

The current study was performed using awake marmosets and a similar methodology as (Sadagopan et al., 2008). Unlike in that study, however, we did not observe a large proportion of nonmonotonic neurons with high best levels. This difference in results may largely be attributable to differences in experimental design. Our design involved a finer sampling of sound levels (10 dB steps as opposed to 20 dB steps), a larger range of sound levels tested (100 dB as opposed to 80 dB) and a longer interval of silence between tone bursts (650 ms as opposed to 300 ms). A diminished range and coarser sampling of sound level could affect the classification of neurons as monotonic or nonmonotonic, which could in turn affect the relative distribution of BL between classifications. Furthermore, as we have reported previously, adaptation produces upward-shifted thresholds in A1 neurons, particularly for monotonic neurons (Watkins et al., 2008; Watkins et al., 2010). Adaptation is strongest at CF, however, and given that tone frequency as well as level was varied in the Sadagopan and Wang study, it seems unlikely that adaptation could affect their results. A coarser sampling of frequency, however (10 frequencies per octave versus 16 frequencies per octave in our study), would likely lead to higher threshold estimates stemming from less accurate CF estimation, particularly for neurons with narrower receptive field bandwidths near threshold. Less accurate CF estimation may also have resulted in a disproportionate number of phasic responses for nonmonotonic neurons (DiMattina et al., 2006). This effect may have contributed to the finding of a significant difference in maximum driven rates between monotonic and nonmonotonic neurons—a difference we did not find in the current study. Both studies did find lower spontaneous spiking in nonmonotonic neurons, however. Finally, the classification into monotonic (i.e., Type I/V) and nonmonotonic (i.e., Type O) neurons differed slightly between the two studies. These distinctions collectively account at least partially for why we observed few nonmonotonic neurons with high thresholds or BLs.

Nonmonotonicity in A1 can be inherited from inputs (Wang et al., 2002; Wehr et al., 2003) or it can be refined or even created locally by combinations of unbalanced excitation and inhibition (Faingold et al., 1991; Sivaramakrishnan et al., 2004; Tan et al., 2007; Wu et al., 2006). Given that this transformation in the neural code appears to occur gradually across multiple auditory stations, level-tuned neurons in auditory cortex seem unlikely to exhibit properties fundamentally different from analogous neurons in subcortical auditory areas. The correlated monotonicity across depth suggests this property is organized within cortical columns, although not with as much organization as frequency. This finding is consistent with previous mapping studies indicating a loosely organized map of monotonicity in A1 (Clarey et al., 1994; Nakamoto et al., 2004; Phillips et al., 1994; Polley et al., 2007; Schreiner et al., 1992) and has implications for the expected topographies of other response features within A1 (Chen et al., 2010; Watkins et al., 2009).

Several hypotheses have been proposed to explain the encoding role of level-tuned neurons. The Best-Intensity Model proposes that nonmonotonic neurons represent a place code for intensity as sounds are transformed along spectral and intensity dimensions (Shamma, 2003). In this model frequency and intensity are encoded over a population of neurons that are narrowly tuned to both stimulus parameters. Studies in the auditory cortex of bats have found evidence for this model, which has been termed an amplitude spectrum representation (Suga, 1977; Suga et al., 1982). These studies also raised the possibility that level-tuned neurons create a “level-tolerant” representation of sounds generally. Later investigation in awake marmoset monkeys reinforced the hypothesis that a major function of nonmonotonic

NIH-PA Author Manuscript

NIH-PA Author Manuscript

NIH-PA Author Manuscript

neurons is to create a level-invariant representation for complex sounds (Sadagopan et al., 2008). The current study did not, however, reveal a uniform distribution of neurons narrowly tuned to intensity, as would be predicted from such models postulating that nonmonotonic neurons represent a place code of intensity. On the other hand, the properties evident in the present study are consistent with other proposed functional schemes of nonmonotonic neurons, including playing a role in the detection of tones in noise (Rees et al., 1988), detecting spectral notches used in sound source localization (Davis et al., 2003; Nakamoto et al., 2004) and discriminating stimulus level (Polley et al., 2006; Polley et al., 2004).

Auditory neurons are known to adapt to statistics of dynamic-level stimuli (Dean et al., 2005; Watkins et al., 2008; Watkins et al.). Responses to tone bursts surrounded by silence, as described in the current study, are also "adapted" responses, but simply adapted to an environment of very low (or silent) sound levels. Previous work in primary auditory cortex has indicated that nonmonotonic neurons do not adapt their input / output functions as much as monotonic neurons in response to dynamic sound level stimuli (Watkins et al., 2008; Watkins et al., 2010). Our results here indicate that nonmonotonic neurons have significantly lower thresholds than monotonic neurons. Thus, nonmonotonic neurons appear to be specialized for encoding low sound levels under silence-adapted as well as dynamic-level conditions.

Supplementary Material

Refer to Web version on PubMed Central for supplementary material.

Acknowledgments

We thank Kim Kocher for valuable assistance with animal training.

Funding

This work was supported by The McDonnell Foundation for Higher Brain Function and the National Institutes of Health grant DC009215.

Abbreviations

A1	primary auditory cortex
BL	best level
CF	characteristic frequency
CN	cochlear nucleus
DCN	dorsal cochlear nucleus
IC	inferior colliculus
MI	monotonicity index
PSTH	peristimulus time histogram
SPL	sound pressure level

References

Abeles M, Goldstein MH Jr. Functional architecture in cat primary auditory cortex: columnar organization and organization according to depth. J Neurophysiol. 1970; 33:172–87. [PubMed: 5411512]

NIH-PA Author Manuscript

NIH-PA Author Manuscript

NIH-PA Author Manuscript

Aitkin L. Rate-level functions of neurons in the inferior colliculus of cats measured with the use of free-field sound stimuli. J Neurophysiol. 1991; 65:383–92. [PubMed: 2016647]

Chen TL, Watkins PV, Barbour DL. Theoretical limitations on functional imaging resolution in auditory cortex. Brain Res. 2010; 1319:175–89. [PubMed: 20079343]

Cheung SW, Bedenbaugh PH, Nagarajan SS, Schreiner CE. Functional organization of squirrel monkey primary auditory cortex: responses to pure tones. J Neurophysiol. 2001; 85:1732–49. [PubMed: 11287495]

Clarey JC, Barone P, Imig TJ. Functional organization of sound direction and sound pressure level in primary auditory cortex of the cat. J Neurophysiol. 1994; 72:2383–405. [PubMed: 7884466]

Davis KA, Ramachandran R, May BJ. Auditory processing of spectral cues for sound localization in the inferior colliculus. J Assoc Res Otolaryngol. 2003; 4:148–63. [PubMed: 12943370]

de la Rocha J, Marchetti C, Schiff M, Reyes AD. Linking the response properties of cells in auditory cortex with network architecture: cotuning versus lateral inhibition. J Neurosci. 2008; 28:9151–63. [PubMed: 18784296]

Dean I, Harper NS, McAlpine D. Neural population coding of sound level adapts to stimulus statistics. Nat Neurosci. 2005; 8:1684–9. [PubMed: 16286934]

DiMattina C, Wang X. Virtual vocalization stimuli for investigating neural representations of species-specific vocalizations. J Neurophysiol. 2006; 95:1244–62. [PubMed: 16207780]

Doron NN, Ledoux JE, Semple MN. Redefining the tonotopic core of rat auditory cortex: physiological evidence for a posterior field. J Comp Neurol. 2002; 453:345–60. [PubMed: 12389207]

Faingold CL, Boersma Anderson CA, Caspary DM. Involvement of GABA in acoustically-evoked inhibition in inferior colliculus neurons. Hear Res. 1991; 52:201–16. [PubMed: 2061208]

Geisler CD, Deng L, Greenberg SR. Thresholds for primary auditory fibers using statistically defined criteria. Journal of the Acoustical Society of America. 1985; 77:1102–9. [PubMed: 3980864]

Heil P, Rajan R, Irvine DR. Topographic representation of tone intensity along the isofrequency axis of cat primary auditory cortex. Hear Res. 1994; 76:188–202. [PubMed: 7928711]

Hromadka T, Deweese MR, Zador AM. Sparse representation of sounds in the unanesthetized auditory cortex. PLoS Biol. 2008; 6:e16. [PubMed: 18232737]

Imaizumi K, Priebe NJ, Crum PA, Bedenbaugh PH, Cheung SW, Schreiner CE. Modular functional organization of cat anterior auditory field. J Neurophysiol. 2004; 92:444–57. [PubMed: 15014102]

Kiang NY, Liberman MC, Levine RA. Auditory-nerve activity in cats exposed to ototoxic drugs and high-intensity sounds. Ann Otol Rhinol Laryngol. 1976; 85:752–68. [PubMed: 999140]

Kiang, NY.; Watanabe, T.; Thomas, EC.; Clark, LF. Discharge Patterns of Single Fibers in the Cat's Auditory Nerve. The MIT Press; Cambridge, MA: 1965a.

Kiang, NYS.; Watanabe, T.; Thomas, EC.; Clark, LF. Discharge Patterns of Single Fibers in the Cat's Auditory Nerve. The MIT Press; Cambridge, MA: 1965b.

Langford E, Schwertman N, Owens M. Is the property of being positively correlated transitive? The American Statistician. 2001; 55:322–325.

Liberman MC. Auditory-nerve response from cats raised in a low-noise chamber. J Acoust Soc Am. 1978; 63:442–55. [PubMed: 670542]

Nakamoto KT, Zhang J, Kitzes LM. Response patterns along an isofrequency contour in cat primary auditory cortex (AI) to stimuli varying in average and interaural levels. J Neurophysiol. 2004; 91:118–35. [PubMed: 14523080]

Nelken I, Young ED. Linear and nonlinear spectral integration in type IV neurons of the dorsal cochlear nucleus. I. Regions of linear interaction. J Neurophysiol. 1997; 78:790–9. [PubMed: 9307113]

Pfingst BE, O'Connor TA. Characteristics of neurons in auditory cortex of monkeys performing a simple auditory task. J Neurophysiol. 1981; 45:16–34. [PubMed: 7205342]

Philibert B, Beitel RE, Nagarajan SS, Bonham BH, Schreiner CE, Cheung SW. Functional organization and hemispheric comparison of primary auditory cortex in the common marmoset (Callithrix jacchus). J Comp Neurol. 2005; 487:391–406. [PubMed: 15906314]

NIH-PA Author Manuscript

NIH-PA Author Manuscript

NIH-PA Author Manuscript

Phillips DP. Neural representation of sound amplitude in the auditory cortex: effects of noise masking. Behav Brain Res. 1990; 37:197–214. [PubMed: 2340096]

Phillips DP, Irvine DR. Responses of single neurons in physiologically defined primary auditory cortex (AI) of the cat: frequency tuning and responses to intensity. J Neurophysiol. 1981; 45:48–58. [PubMed: 7205344]

Phillips DP, Semple MN, Kitzes LM. Factors shaping the tone level sensitivity of single neurons in posterior field of cat auditory cortex. J Neurophysiol. 1995; 73:674–86. [PubMed: 7760126]

Phillips DP, Semple MN, Calford MB, Kitzes LM. Level-dependent representation of stimulus frequency in cat primary auditory cortex. Exp Brain Res. 1994; 102:210–26. [PubMed: 7705501]

Polley DB, Steinberg EE, Merzenich MM. Perceptual learning directs auditory cortical map reorganization through top-down influences. J Neurosci. 2006; 26:4970–82. [PubMed: 16672673]

Polley DB, Read HL, Storace DA, Merzenich MM. Multiparametric auditory receptive field organization across five cortical fields in the albino rat. J Neurophysiol. 2007; 97:3621–38. [PubMed: 17376842]

Polley DB, Heiser MA, Blake DT, Schreiner CE, Merzenich MM. Associative learning shapes the neural code for stimulus magnitude in primary auditory cortex. Proc Natl Acad Sci U S A. 2004; 101:16351–6. [PubMed: 15534214]

Ramachandran R, Davis KA, May BJ. Single-unit responses in the inferior colliculus of decerebrate cats. I. Classification based on frequency response maps. J Neurophysiol. 1999; 82:152–63. [PubMed: 10400944]

Recanzone GH. Response profiles of auditory cortical neurons to tones and noise in behaving macaque monkeys. Hear Res. 2000; 150:104–18. [PubMed: 11077196]

Recanzone GH, Guard DC, Phan ML. Frequency and intensity response properties of single neurons in the auditory cortex of the behaving macaque monkey. J Neurophysiol. 2000; 83:2315–31. [PubMed: 10758136]

Recanzone GH, Schreiner CE, Sutter ML, Beitel RE, Merzenich MM. Functional organization of spectral receptive fields in the primary auditory cortex of the owl monkey. J Comp Neurol. 1999; 415:460–81. [PubMed: 10570456]

Rees A, Palmer AR. Rate-intensity functions and their modification by broadband noise for neurons in the guinea pig inferior colliculus. J Acoust Soc Am. 1988; 83:1488–98. [PubMed: 3372864]

Rhode WS, Smith PH. Characteristics of tone-pip response patterns in relationship to spontaneous rate in cat auditory nerve fibers. Hear Res. 1985; 18:159–68. [PubMed: 2995298]

Rose JE, Greenwood DD, Goldberg JM, Hind JE. Some discharge characteristics of single neurons in the inferior colliculus of the cat. 1. Tonotopic organization, relation of spikes-counts to tone intensity, and firing patterns of single elements. J. Neurophysiol. 1963; 26:295–320.

Ryan A, Miller J. Single unit responses in the inferior colliculus of the awake and performing rhesus monkey. Exp Brain Res. 1978; 32:389–407. [PubMed: 98341]

Sadagopan S, Wang X. Level invariant representation of sounds by populations of neurons in primary auditory cortex. J Neurosci. 2008; 28:3415–26. [PubMed: 18367608]

Schalk TB, Sachs MB. Nonlinearities in auditory-nerve fiber responses to bandlimited noise. J Acoust Soc Am. 1980; 67:903–13. [PubMed: 7358915]

Schreiner CE, Mendelson JR, Sutter ML. Functional topography of cat primary auditory cortex: representation of tone intensity. Exp Brain Res. 1992; 92:105–22. [PubMed: 1486946]

Seiden, HR. Auditory Acuity of the Marmoset Monkey, *Hapale jacchus*. Princeton University; 1957.

Semple MN, Kitzes LM. Single-unit responses in the inferior colliculus: different consequences of contralateral and ipsilateral auditory stimulation. J Neurophysiol. 1985; 53:1467–82. [PubMed: 4009228]

Shamma, SA. Auditory cortex.. In: Arbib, MA., editor. The Handbook of Brain Theory and Neural Networks. 2nd ed.. The MIT Press; Cambridge, MA: 2003. p. 122-127.

Shamma SA, Symmes D. Patterns of inhibition in auditory cortical cells in awake squirrel monkeys. Hear Res. 1985; 19:1–13. [PubMed: 4066511]

NIH-PA Author Manuscript

NIH-PA Author Manuscript

NIH-PA Author Manuscript

Sivaramakrishnan S, Sterbing-D'Angelo SJ, Filipovic B, D'Angelo WR, Oliver DL, Kuwada S. GABA(A) synapses shape neuronal responses to sound intensity in the inferior colliculus. J Neurosci. 2004; 24:5031–43. [PubMed: 15163696]

Spirou GA, Young ED. Organization of dorsal cochlear nucleus type IV unit response maps and their relationship to activation by bandlimited noise. J Neurophysiol. 1991; 66:1750–68. [PubMed: 1765805]

Spirou GA, Davis KA, Nelken I, Young ED. Spectral integration by type II interneurons in dorsal cochlear nucleus. J Neurophysiol. 1999; 82:648–63. [PubMed: 10444663]

Suga N. Amplitude spectrum representation in the Doppler-shifted-CF processing area of the auditory cortex of the mustache bat. Science. 1977; 196:64–7. [PubMed: 190681]

Suga N, Manabe T. Neural basis of amplitude-spectrum representation in auditory cortex of the mustached bat. J Neurophysiol. 1982; 47:225–55. [PubMed: 7062098]

Sutter ML, Schreiner CE. Topography of intensity tuning in cat primary auditory cortex: single-neuron versus multiple-neuron recordings. J Neurophysiol. 1995; 73:190–204. [PubMed: 7714564]

Sutter ML, Loftus WC. Excitatory and inhibitory intensity tuning in auditory cortex: evidence for multiple inhibitory mechanisms. J Neurophysiol. 2003; 90:2629–47. [PubMed: 12801894]

Tan AY, Atencio CA, Polley DB, Merzenich MM, Schreiner CE. Unbalanced synaptic inhibition can create intensity-tuned auditory cortex neurons. Neuroscience. 2007; 146:449–62. [PubMed: 17320296]

Wang J, McFadden SL, Caspary D, Salvi R. Gamma-aminobutyric acid circuits shape response properties of auditory cortex neurons. Brain Res. 2002; 944:219–31. [PubMed: 12106684]

Watkins PV, Barbour DL. Specialized neuronal adaptation for preserving input sensitivity. Nat Neurosci. 2008; 11:1259–61. [PubMed: 18820690]

Watkins PV, Barbour DL. Level-Tuned Neurons in Primary Auditory Cortex Adapt Differently to Loud versus Soft Sounds. Cereb Cortex. 2010 doi: 10.1093/cercor/bhq079.

Watkins PV, Chen TL, Barbour DL. A computational framework for topographies of cortical areas. Biol Cybern. 2009; 100:231–48. [PubMed: 19221784]

Wehr M, Zador AM. Balanced inhibition underlies tuning and sharpens spike timing in auditory cortex. Nature. 2003; 426:442–6. [PubMed: 14647382]

Wu GK, Li P, Tao HW, Zhang LI. Nonmonotonic synaptic excitation and imbalanced inhibition underlying cortical intensity tuning. Neuron. 2006; 52:705–15. [PubMed: 17114053]

Young, E.; Davis, K. Circuitry and function of the dorsal cochlear nucleus.. In: D, O.; RR, F.; AN, P., editors. Integrative functions in the mammalian auditory pathway. Springer-Verlag; New York: 2002. p. 160-206.

Young ED, Brownell WE. Responses to tones and noise of single cells in dorsal cochlear nucleus of unanesthetized cats. J Neurophysiol. 1976; 39:282–300. [PubMed: 1255224]

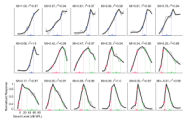

Figure 1.

Normalized rate-level functions from a representative collection of A1 neurons demonstrate the diversity of monotonicity observed in the current study. Neurons in this sample are arranged in order from most monotonic (monotonicity index or MI = 1, upper left) to most nonmonotonic (MI = –0.01, lower right). Rate-level functions were measured with 100 ms tones at CF and are shown as dotted gray lines. Curve fits generated with a six-parameter split-Gaussian model (see Methods) are shown as solid black lines, and the goodness of fit (r^2) for each neuron is indicated. Threshold (20% of maximum) and saturation (80% of maximum) points are labeled on the curves themselves, and dynamic ranges are indicated by horizontal colored lines superimposed onto the sound level axis. Dynamic range midpoints are indicated by colored ticks. For neurons categorized as monotonic (MI > 0.5), only one dynamic range is labeled (blue); whereas for neurons categorized as nonmonotonic (MI ≤ 0.5) a lower dynamic range (red) and an upper dynamic range (green) are labeled separately.

NIH-PA Author Manuscript NIH-PA Author Manuscript NIH-PA Author Manuscript

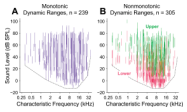

Figure 2.

Dynamic ranges of all neurons in the study population plotted against CF. **A**, Vertical blue lines connect threshold and saturation for monotonic neurons, visually depicting their dynamic ranges. **B**, For nonmonotonic neurons, lower (red) and upper (green) dynamic ranges are depicted separately. Alone, each neuronal subpopulation appears be capable of coding most or all combinations of frequency and intensity. Dependence of threshold upon CF is depicted as a dotted line in both panels. This line provides an estimate of the minimum sensitivity of any neuron at a particular frequency (see Methods).

NIH-PA Author Manuscript
NIH-PA Author Manuscript
NIH-PA Author Manuscript

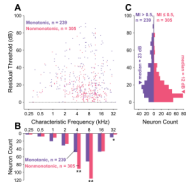

Figure 3.

Comparison of monotonic and nonmonotonic neuron residual thresholds. The residual threshold allows for direct comparison of dynamic ranges across frequency by removing frequency-dependent effects. **A**, Scatterplot of residual thresholds (i.e., neuronal thresholds with frequency-dependent neuronal threshold subtracted) as a function of frequency for monotonic (blue) and nonmonotonic (red) neurons. Overlapping points have their colors superimposed. **B**, Monotonic and nonmonotonic neurons were separately collected into one-octave frequency bins based upon CF to evaluate their relative distribution across frequency. Frequency bins centered at 4 and 8 kHz contained significantly more nonmonotonic than monotonic neurons ($p = 1.7\times10^{-4}$ and $p = 8.2\times10^{-4}$, respectively; binomial test), and the frequency bin centered at 32 kHz contained significantly more monotonic than nonmonotonic neurons ($p = 0.046$, binomial test). These bins are marked with asterisks. **C**, Collapsing residual thresholds across frequency reveals that the distribution of nonmonotonic neurons (median = 12 dB, interquartile range = 15 dB) has a lower central tendency and a smaller range than that of monotonic neurons (median = 23 dB, interquartile range = 28 dB). These two distributions are significantly different ($p = 7.2\times10^{-16}$, Wilcoxon rank sum test).

NIH-PA Author Manuscript NIH-PA Author Manuscript NIH-PA Author Manuscript

NIH-PA Author Manuscript
NIH-PA Author Manuscript
NIH-PA Author Manuscript

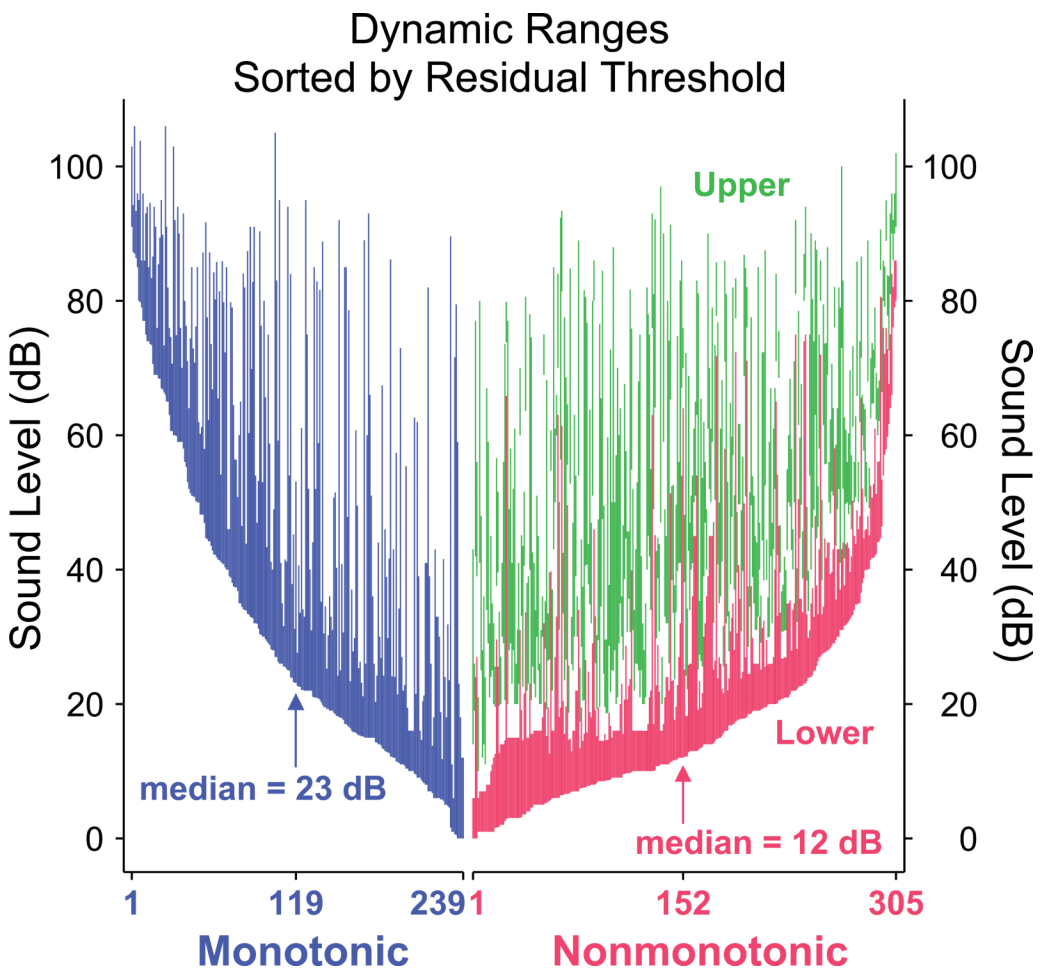

Figure 4.

Monotonic (blue), nonmonotonic lower (red) and nonmonotonic upper (green) dynamic ranges, sorted by residual threshold separately for the monotonic and nonmonotonic populations. Visualizing in this manner shows the clustering of nonmonotonic thresholds closer to the minimum neuronal threshold (at 0 dB residual threshold). Also apparent is that neurons in either population can potentially encode intensities across the entire range of sound levels tested regardless of threshold.

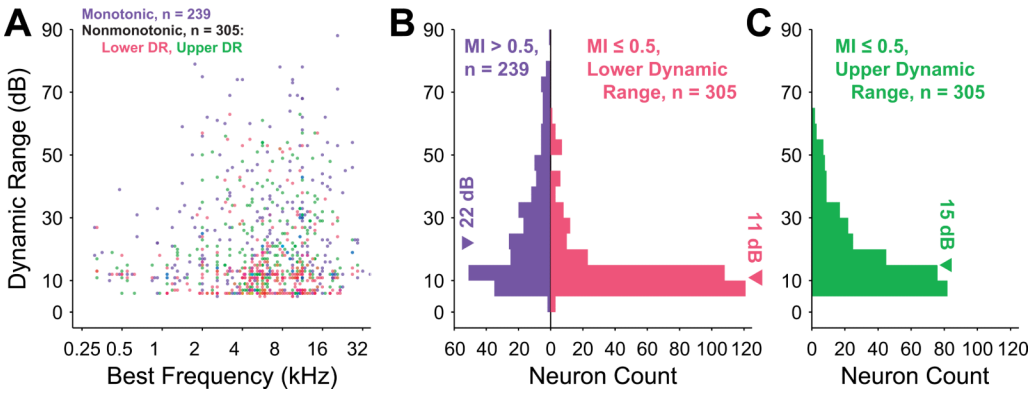

Figure 5.

Dynamic range magnitudes for monotonic neurons (blue) and of lower (red) and upper (green) dynamic ranges for nonmonotonic neurons. **A**, Dynamic ranges as a function of CF reveal that the maximum dynamic range at a particular frequency is limited by the frequency dependence of the thresholds. Overlapping points have their colors superimposed. **B**, Distribution of dynamic ranges for monotonic neurons and of lower dynamic ranges for nonmonotonic neurons reveals a significantly lower median for nonmonotonic neurons ($p = 8.0\times10^{-22}$, Wilcoxon rank sum test). **C**, Median of nonmonotonic upper dynamic range distribution is between the medians given in B and is significantly different from both ($p = 0$, Kruskal-Wallis test with Tukey-Kramer correction for multiple comparisons).

NIH-PA Author Manuscript NIH-PA Author Manuscript NIH-PA Author Manuscript

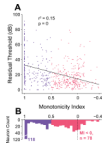

Figure 6.

Residual threshold and monotonicity are correlated. **A**, Scatter plot reveals that the highest residual thresholds are concentrated in the most monotonic subpopulation. Linear regression indicates that threshold and MI are significantly correlated across the entire population (r^2 = 0.15; p = 0, regression F test). Three neurons with MI < –0.4 were not included in the regression and are not depicted in the scatterplot. **B**, Distribution of MI values with a large cluster of very monotonic neurons having MI equal to 1, and a large cluster of neurons having MIs less than or equal to 0.

NIH-PA Author Manuscript
NIH-PA Author Manuscript
NIH-PA Author Manuscript

NIH-PA Author Manuscript
NIH-PA Author Manuscript
NIH-PA Author Manuscript

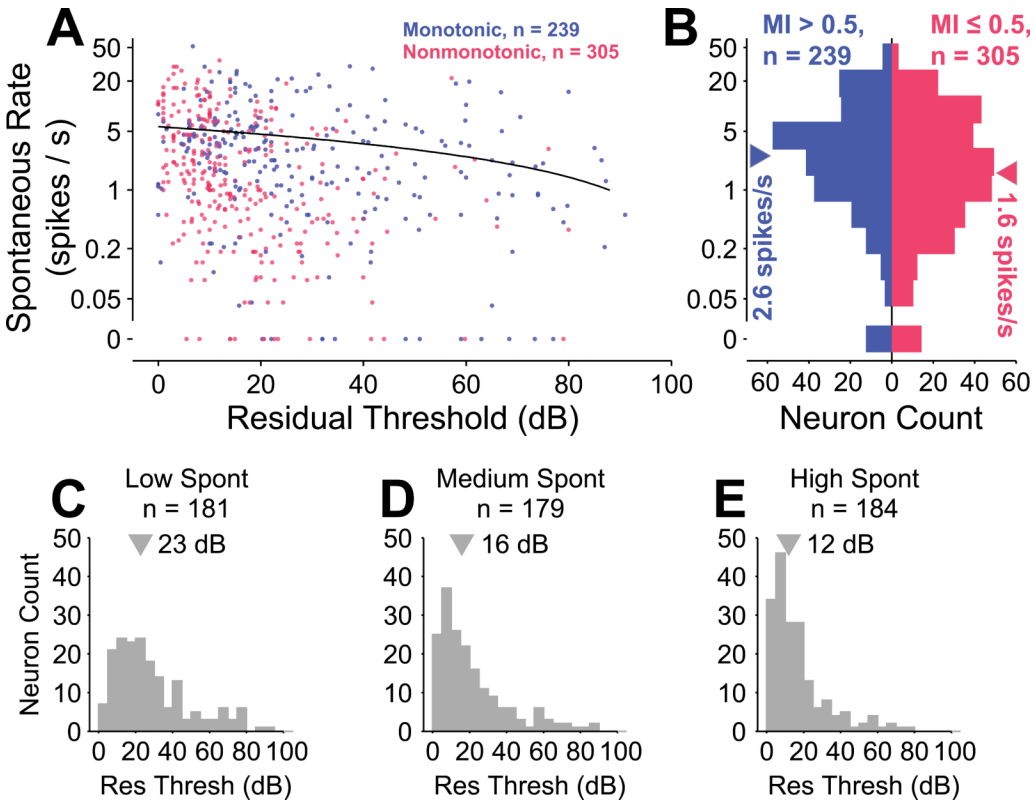

Figure 7.

Spontaneous rate and residual threshold are weakly correlated. **A**, Scatterplot of spontaneous rate versus residual threshold for monotonic (blue) and nonmonotonic (red) neurons reveals that neurons in either population with higher residual thresholds tend to have lower spontaneous rates. Overlapping points have their colors superimposed. A linear regression of this trend reveals a significant, though small effect ($r^2 = 0.026$; $p = 1.5\times10^{-4}$, regression F test). The regression was performed on a linear scale, leading to a curved line on this logarithmic plot. **B**, Collapsing across residual threshold reveals a significant difference between distributions of spontaneous rates for monotonic and nonmonotonic neurons ($p = 0.014$, Wilcoxon rank sum test). **C–E**, Residual threshold differs between groupings into approximate tertiles of spontaneous rate (rate ≤ 0.95, 0.95 < rate ≤ 4, rate > 4).

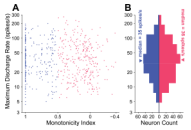

Figure 8.

Maximum discharge rate and monotonicity are not correlated. **A**, Scatterplot of MI versus maximum discharge rate reveals no significant linear trend ($p = 0.13$, Spearman rank correlation test). **B**, Collapsing maximum discharge rate across MI reveals that the monotonic and nonmonotonic populations are not significantly different in maximum discharge rate ($p = 0.48$, Wilcoxon rank sum test).

NIH-PA Author Manuscript
NIH-PA Author Manuscript
NIH-PA Author Manuscript

NIH-PA Author Manuscript

NIH-PA Author Manuscript

NIH-PA Author Manuscript

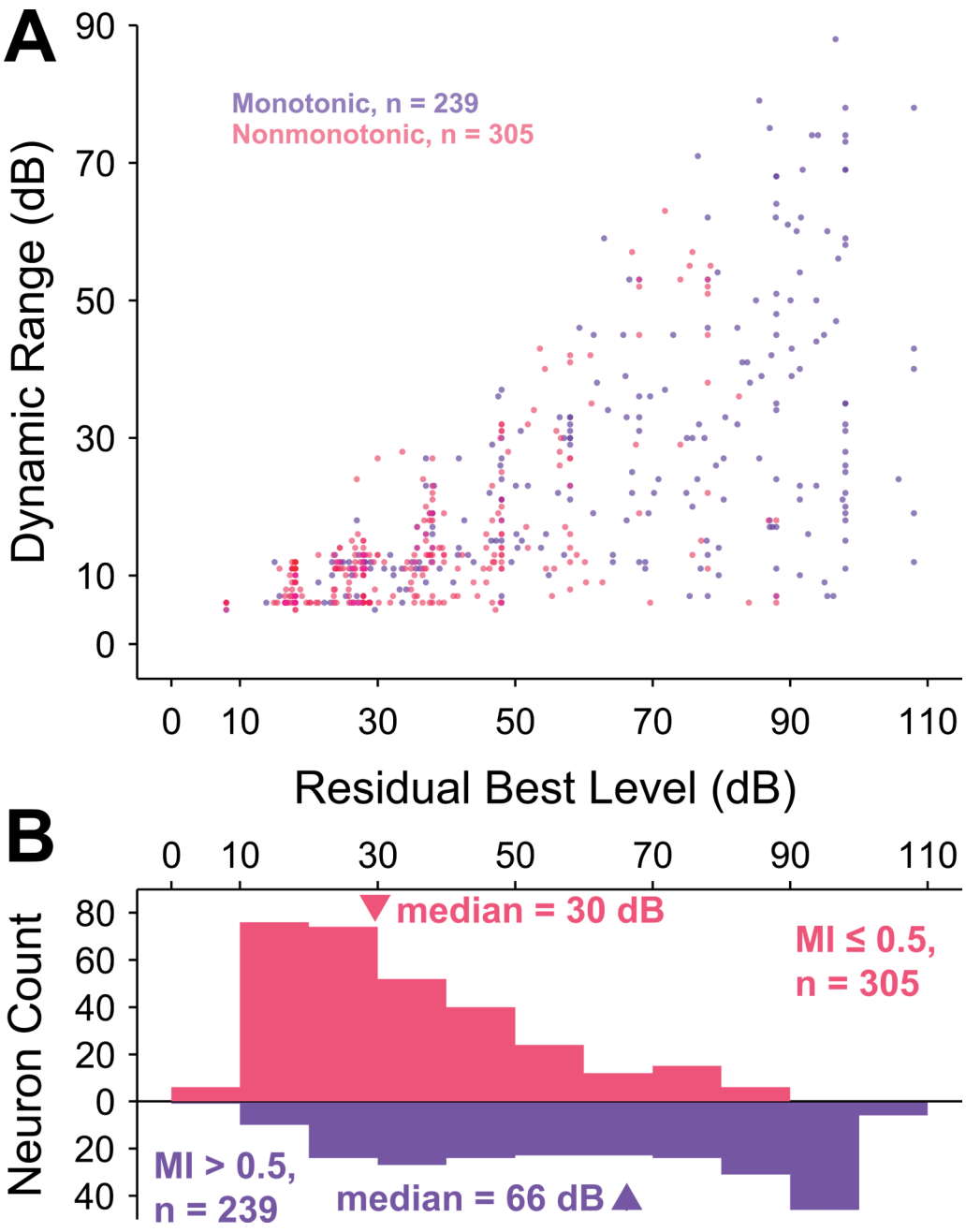

Figure 9.

BL and dynamic range are correlated. **A**, Scatterplot of BL versus dynamic range for monotonic neurons (blue) and lower dynamic range for nonmonotonic neurons (red) reveals an apparent relationship, even though the dynamic range bounds are functions of BL. **B**, The distributions of BL for monotonic and nonmonotonic neurons are significantly different ($p = 3.8\times10^{-32}$, Wilcoxon rank-sum test). The monotonic BL distribution is relatively uniform except for a cluster of neurons with MI equal to 1 (74 / 239), whose BLs are limited by the greatest sound intensity level presented to the neuron. The distribution of BLs for nonmonotonic neurons is skewed towards lower sound levels.

NIH-PA Author Manuscript
NIH-PA Author Manuscript
NIH-PA Author Manuscript

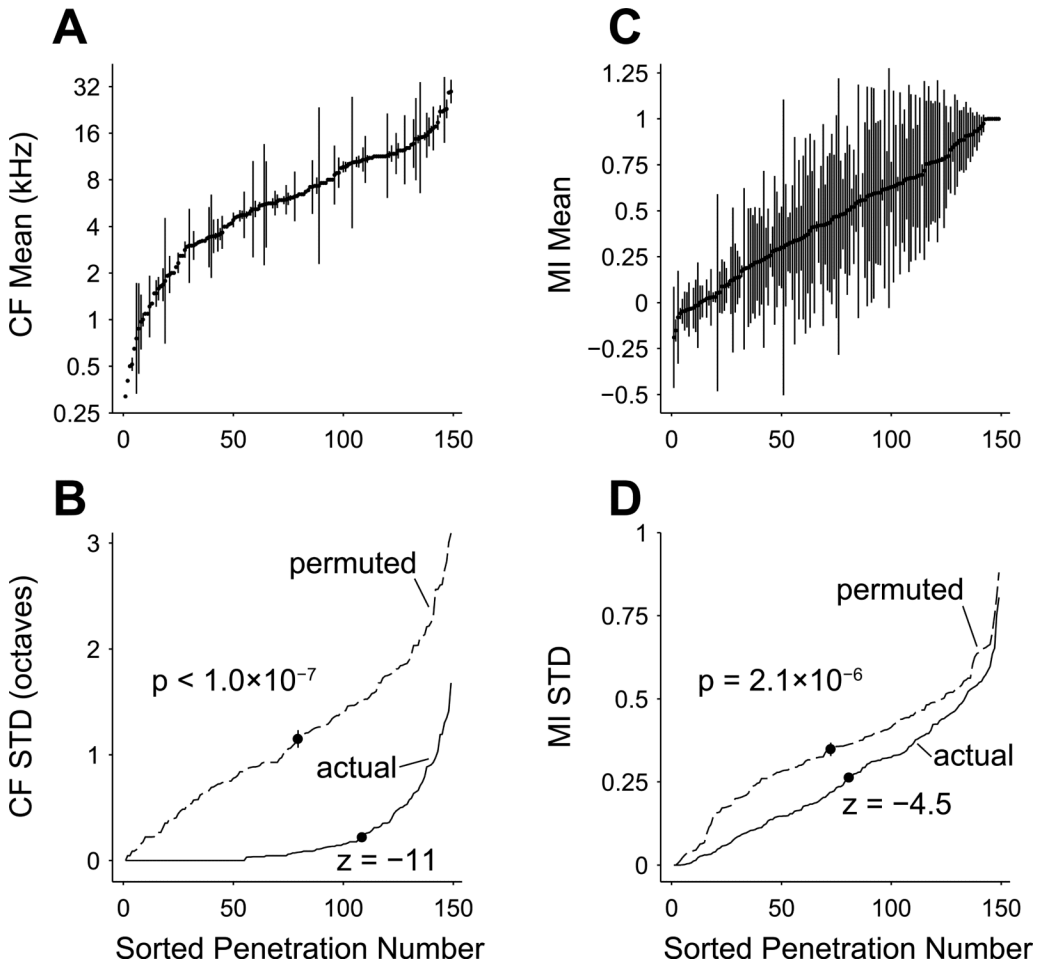

Figure 10.

Neurons are highly organized in columns by CF and loosely but significantly organized in columns by MI. **A**, Electrode penetrations with multiple neurons recorded at different depths are sorted by mean CF. The relatively small standard deviations (errorbars) indicate a high degree of columnar organization of CF ($p < 1.0\times10^{-7}$; permutation test). **B**, When sorted by standard deviation of CF (solid line), the actual penetrations can be seen to have much lower standard deviations than a permuted set of neurons near to the mean of a permutation test statistic distribution (dashed line, see Methods). The mean standard deviation of the penetrations (marked with a dot on the solid line) is significantly different from the mean of the permutation test statistic distribution (marked with a dot on the dashed line; standard deviation marked with errorbar; $z = –11$). **C**, Electrode penetrations sorted by mean MI of the constituent neurons have many more penetrations with large standard deviations as compared to CF (A). Despite this finding, neurons still have a non-random columnar organization of MI ($p = 2.1\times10^{-6}$; permutation test). **D**, Same plot as B, except penetrations are sorted by standard deviation of MI (solid line) and compared with sorted MI standard deviation computed from a permuted set of neurons near to the mean of a permutation test statistic distribution (dashed line). The mean standard deviation of the penetrations (marked with a dot on the solid line) is significantly different from the mean of the permutation test statistic distribution (marked with a dot on the dashed line; standard deviation marked with errorbar; $z = –4.5$).